Identification of four material phases in bitumen by atomic force microscopy

A. Jäger[1], R. Lackner[1], Ch. Eisenmenger-Sittner[2], and R. Blab[3]

[1] *Christian Doppler Laboratory for "Performance-Based Optimization of Flexible Road Pavements"*
Institute for Strength of Materials, Vienna University of Technology
Karlsplatz 13/202, A-1040 Vienna, Austria
Andreas.Jaeger@tuwien.ac.at

[2] *Institute for Solid State Physics, Vienna University of Technology*
Wiedner Hauptstraße 8-10, A-1040 Vienna, Austria

[3] *Christian Doppler Laboratory for "Performance-Based Optimization of Flexible Road Pavements"*
Institute for Road Construction and Maintenance, Vienna University of Technology
Gußhausstraße 28/233, A-1040 Vienna, Austria

ABSTRACT. *The identification of material phases at the so called* bitumen-*scale in context of multiscale modeling of asphalt is presented. For this purpose, atomic force microscopy (AFM), providing insight into the surface topography and mechanical properties, is applied to different types of bitumen. Based on the obtained AFM results, four different material phases at the* bitumen-*scale are identified. These phases are related to the chemical composition of bitumen, characterized by a wide range of molecular mass. Within the anticipated multi-scale model, the properties of these phases serve as input for upscaling, providing material parameter of the bitumen phase at the next-higher scale, i.e., the* mastic-*scale.*

KEYWORDS: *bitumen, multi-scale, atomic force microscopy, pulsed-force mode, non-contact mode.*

Road Materials and Pavement Design. EATA 2004, pages 9 to 24

1. Introduction

Understanding the thermorheological behavior of asphalt is a prerequisite for performance-based optimization of flexible road pavements [BLA 03]. Macroscopic material models for asphalt, describing this thermorheological behavior, are preferably based on temperature-dependent material functions, determined for specific mixture characteristics (aggregate/binder-ratio, type of bitumen and filler) from macroscopic material experiments. In order to account for the wide range of different asphalt mixes, a multiscale model is proposed (see Figure 1). It allows to predict the afore men-

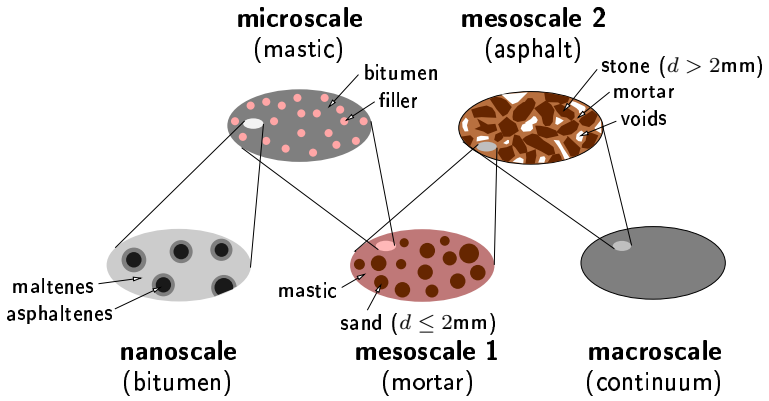

Figure 1. *Multiscale model for determination of temperature-dependent macroscopic material functions*

tioned temperature-dependent material functions by upscaling of information from finer scales of observation towards the *macro*scale. In Figure 1, four additional observation scales are introduced below the *macro*scale, namely (i) the *bitumen*-scale (asphaltene and maltene morphology, see, e.g., [SHE 90]), (ii) the *mastic*-scale (bitumen + filler), (iii) the *mortar*-scale (mastic + aggregate with $d < 2$ mm), and (iv) the *asphalt*-scale (mortar + aggregate with $d > 2$ mm). At each scale of observation, the characteristics (such as structure and material properties) of the constituents present at this scale are obtained either from the next-finer scale via upscaling or need to be specified by respective experiments. Starting from the lowest scale of observation, i.e., the *bitumen*-scale, this paper deals with the identification of structures and material properties at the *bitumen*-scale. In the context of the multiscale model shown in Figure 1, the obtained results will serve as input for upscaling material parameters of bitumen towards the next-higher scale, i.e., the *mastic*-scale.

2. Methods

For the identification of properties at the *bitumen*-scale, the atomic force microscopy (AFM) [BIN 86] is employed. During AFM measurements, the specimen surface

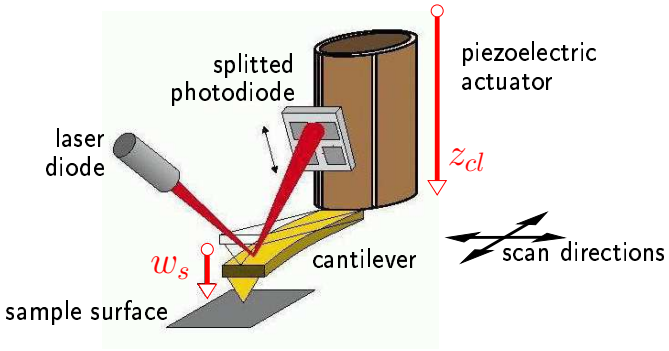

Figure 2. *Principle of AFM measurements (adapted from [SPI 02])*

is scanned by a silica or silica-nitride cantilever with a small tip (AFM tip) at the free end (see Figure 2). The deflection w_s of the cantilever is detected by an optical lever method [ALE 89]. Based on w_s, a picture representing properties at the specimen surface is obtained. Hereby, depending on the mode of measurement (non-contact versus pulsed-force mode), either the surface topography or the near-surface mechanical properties of bitumen can be identified. The results presented in this paper were obtained from the AFM *Topometrix Explorer* [TOP 96].

2.1. *Non-contact mode (NCM)*

During AFM measurements employing the NCM, the oscillation of the AFM cantilever, described by the amplitude corresponding to free oscillation A_0 [V], is reduced by attraction/repulsive forces when approaching the bitumen surface. By enforcing a constant reduction of the amplitude, with e.g. $A_{sp}/A_0 = 0.5$, where A_{sp} represents the amplitude of the near-surface oscillation, an image of the surface topography is obtained. Using the mentioned AFM equipment, these measurements were conducted with a frequency f [Hz] equal to the resonance frequency of the cantilever, with $f = 270$ kHz.

2.2. *Pulsed-force mode (PFM)*

In contrast to the NCM, the tip located at the end of the cantilever is penetrating the specimen surface during PFM measurements, providing insight into mechanical properties of bitumen. By reducing the frequency f from 270 kHz (NCM) to 0.1 – 2 kHz, the deflection of the cantilever, w_s [nm] (solid line in Figure 3), is recorded. Based on the deflection history depicted in Figure 3, two output quantities are provided by the AFM [WIT 02]:

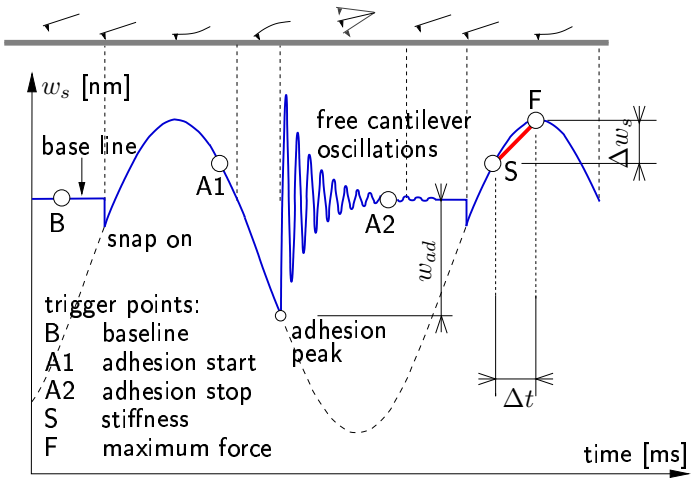

Figure 3. *Deflection of the cantilever (solid line) during PFM measurements (adapted from [WIT 02])*

– V_s [V] describes the history of the recorded signal between the points S and F (see Figure 3). These points are placed by the user within the time domain characterized by penetration of the tip into the bitumen (according to [WIT 02], F should be placed at the maximum value).

– V_{ad} [V] is the output value corresponding to the minimum deflection monitored between the time interval defined by the user-defined points $A1$ and $A2$ (see "adhesion peak" in Figure 3).

Based on the values of V_s and V_{ad}, the deflection increment between S and F, Δw_s, and the deflection at the "adhesion peak", w_{ad}, of the cantilever can be computed as

$$\Delta w_s = \frac{V_s\, C}{S\, g_s} \quad \text{and} \quad w_{ad} = \frac{V_{ad}\, C}{S\, g_{ad}}\,, \qquad [1]$$

where $C = 6.4$ nA/V is a constant [WIT 02], S is the sensitivity of the photo diode, which was ranging from 0.036 to 0.040 nA/nm, $g_s = 1$ and $g_{ad} = 1$ are amplification factors. Employing the stiffness k [N/m] of the cantilever, with $k = 2.5$ N/m [TOP 96], the force increment between F and S, ΔF_s, and the force at the "adhesion peak", F_{ad}, are obtained as

$$\Delta F_s = k\, \Delta w_s \quad \text{and} \quad F_{ad} = k\, w_{ad}\,. \qquad [2]$$

In order to relate ΔF_s and F_{ad} to mechanical properties of the tested material, four theories can be distinguished:

– In the **Hertz model** [HER 81], the contact between two elastic spheres is considered. In case of the AFM, the radius of one sphere (material sample) is infinite,

whereas the radius of the other sphere is set equal to the radius of the AFM tip. Since no adhesion is considered in the Hertz model, it may be employed only in case of large forces F and negligible surface forces.

– In the **JKR model** [JOH 71], the Hertz model was extended to consideration of surface forces. It gives good results for large tip radii and soft materials.

– In the **DMT model** [DER 75], the surface forces acting outside the contact area are taken into account. Accordingly, the singularity observed at the boundary of the contact surface in the JKR model is eliminated. However, no deformation of the surface in consequence of adhesion forces is taken into account. Hence, it may only be used for materials with low adhesion.

– Finally, the **Maugis model** [MAU 92] is the most general model, being applicable to soft materials with high surface forces and rigid materials with low surface forces. A dimensionless parameter λ, related to the size of the neck forming in consequence of adhesive forces, is introduced [CAP 99] [ROS 97]. The Maugis model reduces to the DMT model for $\lambda \to 0$ and to the JKR model for $\lambda \to \infty$.

For the determination of mechanical properties of bitumen, characterized by large surface forces, the JKR model is employed. In the following, this model is described in more detail.

2.2.1. *Determination of surface energy W [Nm/m^2] of bitumen*

According to [JOH 71], the surface energy can be extracted from

$$F_{ad} = -\frac{3}{2}\pi\, R\, W\ , \qquad [3]$$

where R represents the radius of the AFM tip, which can be obtained from scanning of special test samples [BYK 03].

2.2.2. *Determination of stiffness properties of bitumen*

Within the JKR model, the penetration depth z [nm] is related to the radius a [nm] of the contact area between the AFM tip and the bitumen as

$$z(a) = \frac{a^2}{R} - \frac{2}{3}\sqrt{\frac{6\,\pi\, W\, a}{K}}\ , \qquad [4]$$

where K [N/m^2], representing the reduced Young's modulus, is obtained from inserting [CAP 99]

$$a = \sqrt[3]{\frac{R}{K}\left[F_s + 3\pi RW + \sqrt{6\pi RW F_s + (3\pi RW)^2}\right]}\ , \qquad [5]$$

into Equation (4). In Equation (5), F_s is the applied force computed from the cantilever stiffness k and the corresponding deflection of the cantilever, w_s. Finally, knowledge of K and assuming that Young's modulus of the AFM tip is much higher than that of bitumen, Young's modulus E of bitumen is obtained as [CAP 99]

$$E = \frac{3}{4}(1-\nu^2)K\ , \qquad [6]$$

with ν as the Poisson's ratio.

Since only the force increment, ΔF_s, is available from the PFM measurements and, hence, the radius a of the contact area in Equation (5) cannot be computed, a secant stiffness K_T, defined as

$$K_T = \frac{\Delta F_s}{\Delta z} \,, \qquad [7]$$

is introduced. In Equation (7), the penetration Δz is obtained from the difference between the respective vertical displacement increment of the cantilever, Δz_{cl}, and the deflection increment Δw_s (Equation (1)). Δz_{cl} can be computed from

$$\Delta z_{cl} = M_{cl} \times [1 - \cos(2\pi\, f\, \Delta t)] \,, \qquad [8]$$

with M_{cl} as the amplitude of the cantilever during AFM testing, and f [kHz] as the frequency. Δt [ms] refers to the time span between F and S, ranging between 0.17 and 0.18 ms (see Figure 3).

2.3. *Cooling stage*

In the course of PFM testing, the low viscosity of bitumen caused severe problems in the performance of the AFM (parts of the bitumen sticked onto the tip of the cantilever). In order to increase the viscosity of bitumen, a cooling stage consisting of a Peltier element (PEL 169), placed on a copper block was installed (see Figure 4). The copper block with the Peltier element on its top surface was put in a water bath, allowing to compensate the heat produced at the bottom, while cooling the bitumen specimen at the top of the Peltier element (see Figure 4).

3. Materials

In order to cover a wide range of different bitumen, five types of bitumen with varying penetration depths were considered for the study (see Table 1). Whereas B50/70,

Table 1. *Characteristics of the bitumens used in this study (parameters according to [ÖNORM EN 12593 00] [ÖNORM EN 1427 00] [ÖNORM EN 1426 00])*

	B160/220	B70/100	EL60/90	B50/70	B90/10
penetration depth [1/10 mm]	151	72	64	49	7
breaking point by Fraaß [°C]	-17	-17	-18	-13	4
softening point [°C]	40	47	58	51	87

B70/100, and B160/220 are standard bitumen, B90/10 was hardened by means of air-blowing and EL60/90 was modified by the allowance of styrene-butadiene-styrene (SBS).

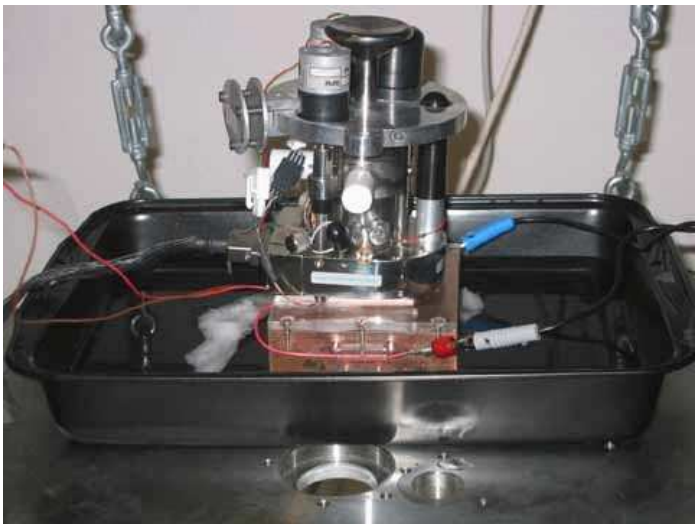

Figure 4. *Cooling stage for AFM testing consisting of Peltier element (PEL 169), a copper block, and a water bath, with the AFM on the top*

For AFM testing, the specimens were melted, allowing the bitumen to be poured into sample holders, made of steel with a diameter of 2 cm. The time span between specimen preparation and AFM testing was approximately seven days, eliminating influences resulting from physical and steric hardening [MAS 01].

4. Presentation of results

4.1. *Results from NCM testing*

Figure 5 shows AFM plots from NCM measurements of B50/70 and B160/220 at room temperature (no cooling). Similar to experimental results presented in [LOE 96], randomly distributed "bee-shaped" structures are observed for both types of bitumen. The impression of "bees" stems from alternating higher and lower parts of the surface topography of bitumen. In the following presentation, the bitumen surface is divided

	B160/220	B70/100	EL 60/90	B50/70	
plot range [nm]	250	158	136	162	
d [nm]	600	550	470	550	$\approx$550

Table 2. *Characteristic dimensions of "bees" obtained from NCM experiments (plot range correlates to topographical change ΔH within "bees")*

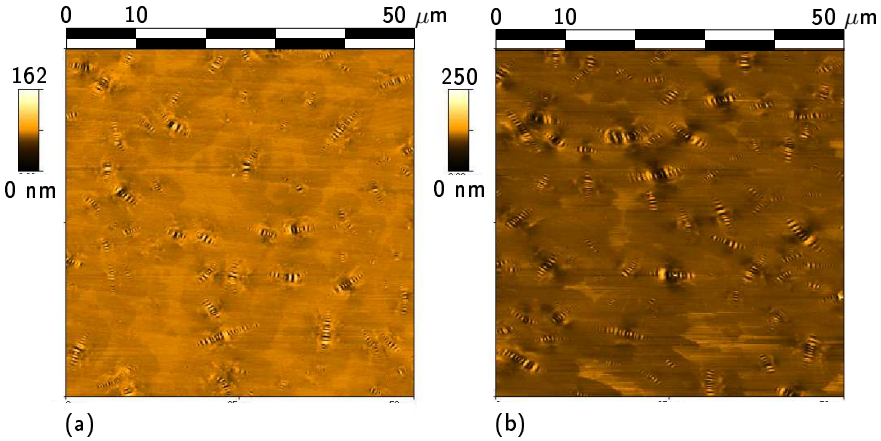

Figure 5. *NCM result for (a) B50/70 and (b) B160/220 obtained from NCM ($A_0 = 0.04\,V$ and $A_{sp}/A_0 = 0.5$)*

into two phases, i.e., the "bee-shaped" structures and the matrix phase surrounding the "bee-shaped" structures. Within the matrix, two subdomains characterized by a difference in the topography of 5 nm can be distinguished. The lower part of the matrix is arranged around the "bee-shaped" structures, whereas the higher parts of the matrix are found at larger distance from the "bees". Hence, four phases, i.e., the lower and the higher parts in both the "bees" and the matrix were identified by the NCM measurements.

In addition to the images given in Figure 5, the AFM gives access to characteristic dimensions of the topographical structures. Figure 6 shows a section through a "bee", illustrating the earlier mentioned higher and lower parts within the "bee-shaped" structure. The two quantities describing the "bee-shaped" structure, i.e., the maximum topographical change ΔH (correlated with the plot range of the NCM images, see e.g. Figure 5) and the distance between the higher parts of "bees", d, are summarized in Table 2 for different types of bitumen. Whereas no correlation is found between the type of bitumen and the plot range, the distance d between the higher parts in the "bee-shaped" structure is approximately the same for all bitumen, namely 550 nm. This is in agreement with the experimental data given in [LOE 96], having observed strips (corresponding to the higher parts of the "bees" found in the present results) with a thickness of 100 to 200 nm.

In order to assess whether or not the material phases identified by NCM testing possess different mechanical properties, PFM measurements were conducted. The obtained results are presented in the following.

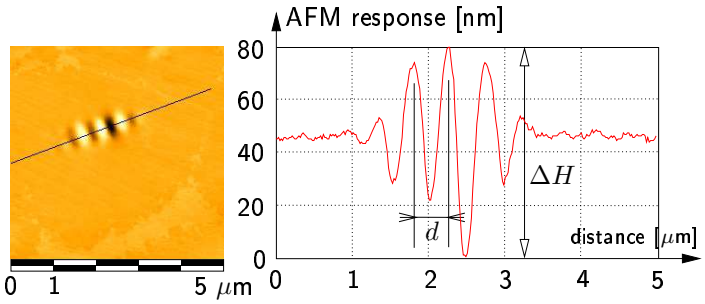

Figure 6. *Characteristic dimensions d [nm] and ΔH [nm] of one "bee"*

4.2. *Results from PFM testing*

Figure 7 shows plots of the output quantities V_s and V_{ad} obtained from PFM measurements for B70/100 at $T = 10°$C. According to these results, the four subdomains identified from the surface topography in the previous subsection exhibit different mechanical properties. Hereby, the parts of the surface with larger stiffness (see light areas in Figure 7(a)) show a lower adhesive behavior, and vice versa. E.g., the value of V_{ad} for the stiffer part of the matrix around the "bees" is lower than V_{ad} in the softer part of the matrix.

Based on the same value for the setpoint (SP), defining the penetration depth of the AFM tip, the PFM experiment was repeated for B50/70 (see Figure 8). Again, the four phases can be identified. However, since the PFM experiment of the B50/70 was

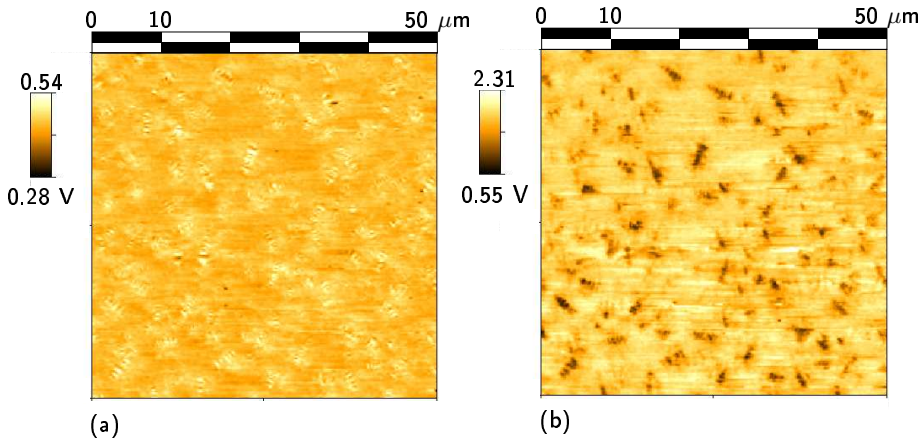

Figure 7. *PFM plots showing (a) V_s [V] and (b) V_{ad} [V] of B70/100 ($SP = 3$ nA, $T = 10°C$, $f = 306$ Hz)*

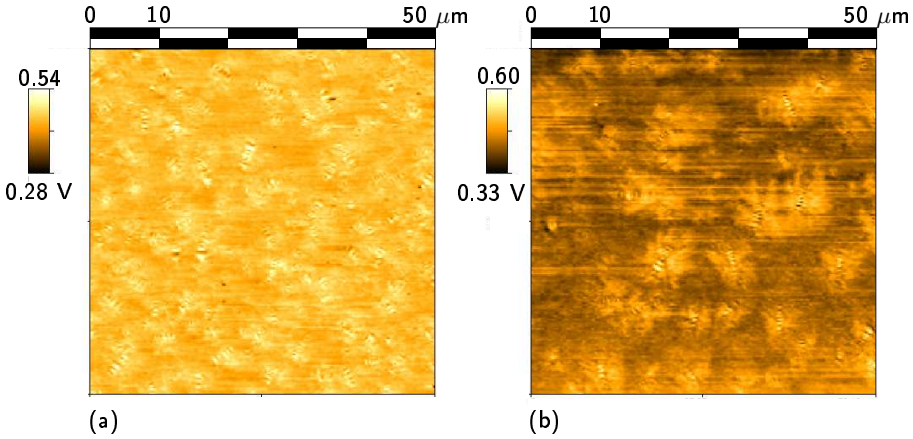

Figure 8. *PFM plots showing V_s [V] of (a) B70/100 ($T = 10°C$) and (b) B50/70 ($T = 15°C$) ($SP = 3$ nA, $f = 306$ Hz)*

performed at $T = 15°$C, the amount of the matrix characterized by lower stiffness increased. In order to gain insight into the stiffness properties of the four subdomains observed for both bitumen shown in Figure 8, the relative stiffness, determined from averaging the value of V_s over selected parts of the PFM plots, are given in Figure 9. The values corresponding to the soft matrix and the soft part of the "bees" are al-

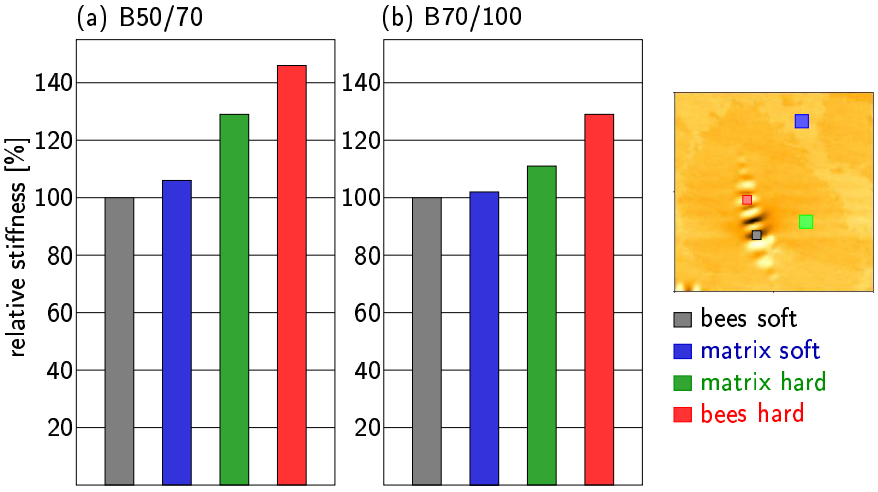

Figure 9. *Relative stiffness of the four phases of B70/100 and B50/70 determined from V_s plots*

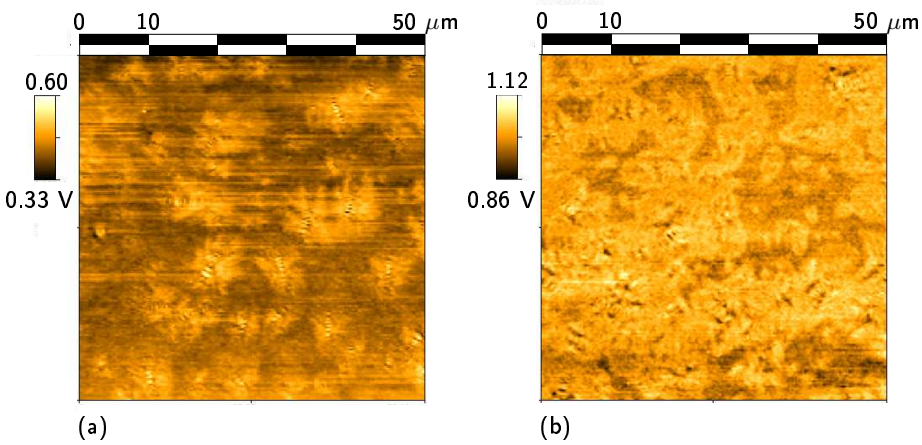

Figure 10. *PFM plots showing V_s [V] of B50/70 using (a) $SP = 3$ nA, and (b) $SP = 10$ nA ($T = 15°C$, $f = 306$ Hz)*

most the same. However, they were obtained from different parts of the PFM plots, separated by the hard-matrix phase.

Figure 10 shows PFM results for B50/70 using two different SPs, i.e., for two different penetration depths. By increasing the SP from 3 to 10 nA, the rather local hard-matrix phase surrounding the "bees" becomes interconnected.

5. Discussion

Whereas AFM results provide quantitative data regarding the dimensions of the identified material phases at the *bitumen*-scale (Figure 6), reflected-light-microscope (RLM) images, such as shown in Figure 11, give a more detailed insight into the structures at the bitumen surface of the different material phases. Similar to the AFM results, the RLM images show "bee-shaped" structures. According to Figure 11, these "bees" serve as nuclei for further arrangement of molecules, building up the earlier-identified hard-matrix phase. In order to assess the chemical composition of the "bee-shaped" structures and the hard-matrix phase, the asphaltenes were precipitated by the addition of n-heptane. In contrast to the images shown in Figure 11, the so-obtained phase, also referred to as maltene phase, exhibits neither "bees" nor a hard-matrix phase (see Figure 12). The slightly darker parts in Figure 12 are air inclusions resulting from pouring of the maltene phase into the sample holder. Based on these results, the formation of "bees" and the hard-matrix at the bitumen surface can be related to the presence of asphaltenes.

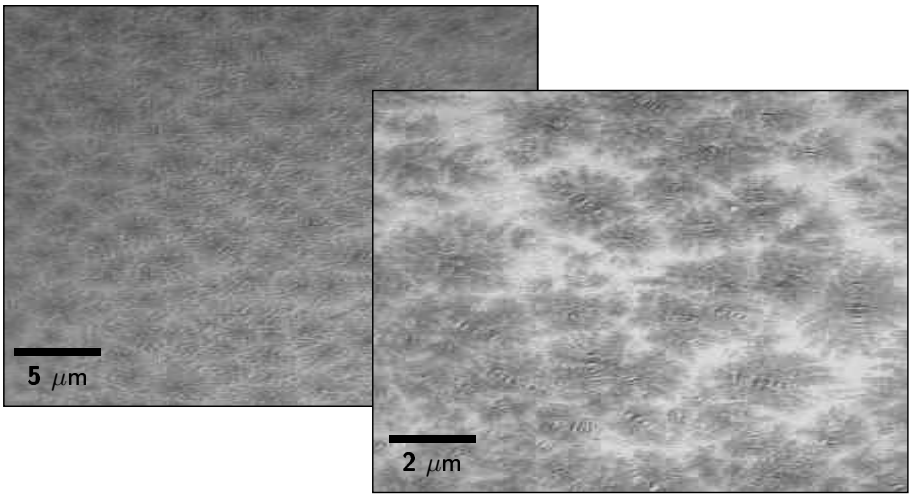

Figure 11. *Reflected-light-microscope image of bitumen surface*

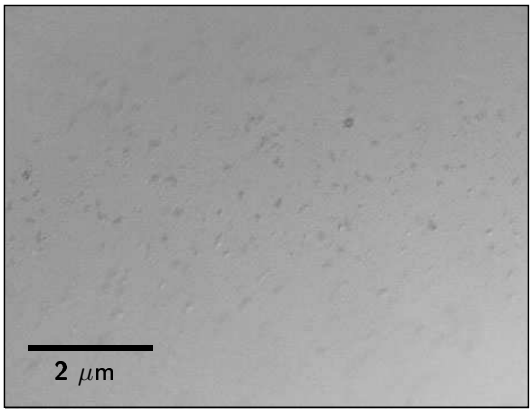

Figure 12. *Reflected-light-microscope image of bitumen (asphaltenes precipitated by the addition of n-heptane)*

In the literature, bitumen is described as a colloidal system of asphaltene micelles, surrounded by an absorbed sheath of high-molecular-weight resins, dispersed in a low-molecular-weight oily medium [HOB 84, SHE 90, STE 92]. According to [SHE 90], the formed microstructure in bitumen depends on the amount of resins and aromatics, giving either fully-peptized micelles (sol-like structure) or micelles irregularly packed within an open structure (gel-like structure). The formation of a microstructure by the arrangement of molecules was identified by endotherms in the non-reversing heat flow in modulated differential scanning calorimetry (MDSC) measurements (see

[MAS 01, MAS 02, JÄG 04]). The dis-arrangement of molecular structures associated with these endotherms continues until the temperature reaches 90 °C [JÄG 04].

Considering the micelles surrounded by high-molecular-weight resins as primary "building unit" of the bitumen microstructure, both asphaltenes and resins may be present in the the "bees" and the hard-matrix phase observed in Section 4. This also agrees with the higher stiffness in these parts at the bitumen surface measured during PFM testing (see Figures 7 and 8). According to [SHE 90], the large polarity of asphaltenes and resins explains the higher stiffness in these parts of bitumen observed during PFM testing.

Local "bee"-shaped or network structure?

The still unanswered question concerns the existence of "bee-shaped" structures in bitumen. From the PFM results using a larger set point SP, i.e., increasing the penetration of the AFM tip into the bitumen, the stiffer parts of the matrix became interconnected, suggesting that the "bees" observed during NCM testing belong to network structure, emerging and immersing at the bitumen surface. [LOE 96] reports on a similar three-dimensional network observed during AFM measurements on bitumen by scanning the surface at constant height and recording the force variation. In [LOE 96], the formation of the network is explained by the arrangement of asphaltenes and resins, while the remaining part is referred to as oily phase. A similar network structure, however, obtained from a different experimental technique, was identified by [ROZ 97] using an environmental scanning electron microscope (ESEM). Hereby, the small-size molecules at the bitumen surface were evaporated, enabling the view onto a network entanglement of strands.

Having identified the "bees" as part of a network structure emerging and immersing from the bitumen surface, the fact of alternating topography (high and low areas separated by approximately 275 nm) is still unanswered. In contrast to the spherical shape of micelles reported in the open literature, the different radii in direction and perpendicular to the direction of the "bee-shaped" structure suggest a building unit with an oblate-spheroid shape. However, the size of this spheroid, corresponding to the radii measured during NCM testing, is significantly larger than the dimensions of micelles given in the literature (100 nm [LOE 96], 20 nm and 1.2 μm [ROZ 97]).

Conclusions and outlook on future work

The AFM was successfully employed for the identification of material phases at the *bitumen*-scale. Four material phases were encountered at the bitumen surface:

1) The *hard-bee* phase is part of the "bee-shaped" structure, presumably containing high polar molecules, such as asphaltenes and resins.

2) The *hard-matrix* phase results from the arrangement of molecules originating from the "bees".

3) The *soft-matrix* phase is the part which, at a certain temperature, does not show any arrangement of molecules. In this phase, low stiffness and high surface forces were encountered.

4) The *soft-bee* phase is responsible for the impression of "bees" at the bitumen surface. Surprisingly, the distance between two soft-bee phases is approximately 550 nm, independent of the type of bitumen.

In addition to the identification of material phases, the use of the PFM provided insight into the structure of the bulk of bitumen, showing a network structure consisting of the "bee" phases surrounded by a hard-matrix phase.

In order to gain more insight into the properties of the bitumen bulk, additional NCM measurements characterized by a modified sample preparation (low-temperature cracking instead of pouring of bitumen) will be conducted. Moreover, the PFM measurements reported in this paper will be replaced by nano indentation, allowing to perform creep and relaxation tests with pre-specified load history over a wide temperature range.

Both the mechanical properties obtained from PFM testing (and the future results from nano indentation) as well as the identified microstructure of bitumen will serve as input for upscaling within the multi-scale model, finally providing insight into the effect of the bitumen microstructure on the macroscopic properties of the bitumen-aggregate composite, the asphalt.

Acknowledgements

The authors thank the remaining members of the Christian Doppler laboratory, especially Michael Kostjak (Swietelsky, Austria) and Andreas Loibl (OMV, Austria) for helpful comments and fruitful discussions on the presented research work. The authors are indebted to Andrea Jauss and Peter Spizig (Witec, Germany) for helpful support in the course of PFM test. Financial support by the Christian Doppler Gesellschaft is gratefully acknowledged.

6. References

[ALE 89] ALEXANDER S., HELLEMANS L., MARTI O., SCHNEIR J., ELINGS V., HANSMA P., LONGMIRE M., GURLEY J., "An atomic-resolution atomic-force microscope implemented using an optical lever", *Journal of Applied Physics*, vol. 65, 1989, p. 164–167.

[BIN 86] BINNIG G., QUATE C., GERBER C., "Atomic force microscope", *Physical Review Letters*, vol. 56, num. 9, 1986, p. 930–933.

[BLA 03] BLAB R., "Gebrauchsverhaltensorientierte Optimierung flexibler Straßenbefestigungen [Performance-based optimization of flexible road pavements]", report, June 2003, Department of Civil Engineering, Vienna University of Technology, Vienna, Austria, In German.

[BYK 03] BYKOV V., NOVIKOV Y., RAKOV A., S.M. S., "Defining the parameters of a cantilever tip AFM by reference structure", *Ultramicroscopy*, vol. 96, 2003, p. 175–180.

[CAP 99] CAPPELLA B., DIETLER G., "Force-distance curves by atomic force microscopy", *Surface Science Reports*, vol. 34, 1999, p. 1–104.

[DER 75] DERJAGUIN B., MULLER V., TOPOROV Y., "Effect of contact deformations on the adhesion of particles", *Journal of Colloid and Interface Science*, vol. 53, num. 2, 1975, p. 314–326.

[HER 81] HERTZ H., "Über die Berührung fester elastischer Körper [On the contact of solid elastic bodies]", *Journal für die reine und angewandte Mathematik*, vol. 92, 1881, p. 156–171.

[HOB 84] HOBSON G., *Modern petroleum technology, Part II*, vol. 5, The Institute of Petroleum, London, England, 1984.

[JÄG 04] JÄGER A., "Microstructural identification of bitumen by means of atomic force microscopy (AFM), modulated differential scanning calorimetry (MDSC), and reflected light microscopy (RLM)", Master's thesis, Vienna University of Technology, Vienna, 2004.

[JOH 71] JOHNSON K., KENDALL K., ROBERTS A., "Surface energy and the contact of elastic solids", *Proc. R. Soc. Lond*, vol. A324, 1971, p. 301–313.

[LOE 96] LOEBER L., SUTTON O., MOREL J., VALLETON J.-M., MULLER G., "New direct observations of asphalt and asphalt binders by scanning electron microscopy and atomic force microscopy", *Journal of Microscopy*, vol. 182, 1996, p. 32–39.

[MAS 01] MASSON J.-F., POLOMARK G. M., "Bitumen microstructure by modulated differential scanning calorimetry", *Thermochimica acta*, vol. 374, 2001, p. 105–114.

[MAS 02] MASSON J.-F., POLOMARK G. M., COLLINS P., "Time-dependent microstructure of bitumen and its fractions by modulated differential scanning calorimetry", *Energy and Fuels*, vol. 16, 2002, p. 470–476.

[MAU 92] MAUGIS D., "Adhesion of spheres: The JKR-DMT transition using a Dugdale model", *Journal of Colloid and Interface Science*, vol. 150, num. 1, 1992, p. 243–269.

[ÖNORM EN 12593 00] ÖNORM EN 12593, "Bitumen und bitumenhaltige Bindemittel – Bestimmmung des Brechpunktes nach Fraaß [Bitumen and bituminous binders – Determination of the Fraass breaking point]", Österreichisches Normungsinstitut, Vienna, 2000, In German.

[ÖNORM EN 1426 00] ÖNORM EN 1426, "Bitumen und bitumenhaltige Bindemittel – Bestimmmung der Nadelpenetration [Bitumen and bituminous binders – Determination of needle penetration]", Österreichisches Normungsinstitut, Vienna, 2000, In German.

[ÖNORM EN 1427 00] ÖNORM EN 1427, "Bitumen und bitumenhaltige Bindemittel – Bestimmmung des Erweichungspunktes – Ring- und Kugel-Verfahren [Bitumen and bituminous binders – Determination of softening point - Ring and Ball method]", Österreichisches Normungsinstitut, Vienna, 2000, In German.

[ROS 97] ROSA-ZEISER A., "Der Pulsed Force Mode als kraftmikroskopische Untersuchungsmethode für unterschiedlich gefüllten Naturkautschuk bei linearer Deformation [The pulsed force mode as force microscopical examination method for variable filled natural rubber at linear deformation]", Master's thesis, University of Ulm, Ulm, 1997, In German.

[ROZ 97] ROZEVELD S., SHIN E., BHURKE A., FRANCE L., DRZAL L., "Network morphology of straight and polymer modified asphalt cements", *Microscopy Research and Technique*, vol. 38, 1997, p. 529–543.

[SHE 90] SHELL-BITUMEN-U.K., *The Shell bitumen handbook*, vol. 1, Shell Bitumen UK, Chertsey, 1990.

[SPI 02] SPIZIG P., "Dynamische Rasterkraftmikroskopie [Dynamic atomic force microscopy]", Master's thesis, University of Ulm, Ulm, 2002, In German.

[STE 92] STEIDL E., "Studien über den Nachweis von Styrol-Butadien-Copolymeren in Bitumen und deren Wechselwirkungen mit Bitumen [Studies on the existance of styrene-butadiene-copolymers in bitumen and their interaction with bitumen]", Master's thesis, Vienna University of Technology, Vienna, 1992, In German.

[TOP 96] TOPOMETRIX, "Explorer instrument operation manual", TopoMetrix Corporation, Santa Clara, 1996.

[WIT 02] WITEC, "Pulsed force mode", WITec GmbH., Ulm, 2002.